

## RIETVELD REFINEMENT OF CLINOPYROXENES WITH INTERMEDIATE Ca-CONTENT ALONG THE JOIN DIOPSIDE–ENSTATITE

MARIO TRIBAUDINO<sup>§</sup>

*Dipartimento di Scienze della Terra, Università di Parma, Parco Area delle Scienze 157/A, I-43100 Parma, Italy*

FABRIZIO NESTOLA<sup>§</sup>

*Bayerisches Geoinstitut, Universität Bayreuth, D-95440 Bayreuth, Germany*

CARLO MENEGHINI<sup>§</sup>

*Dipartimento di Fisica “E. Amaldi”, Università di Roma 3, Via della Vasca Navale 84, I-00146 Roma, Italy*

### ABSTRACT

The structures of five clinopyroxenes on the diopside–enstatite join have been refined by Rietveld analysis of powder-diffraction patterns obtained with synchrotron radiation. The reliability of the present Rietveld refinements was checked against previous single-crystal data on the sample with composition  $\text{Di}_{80}\text{En}_{20}$ , and it showed reasonable agreement. A difference in the  $y/b$   $M2$  coordinate is related to the lower resolution of the powder-diffraction data of this work, not sufficient to detect the splitting at the  $M2$  site. The Rietveld analysis allowed us to detect the strain modulations on (010) prior to exsolution. The small size of primitive antiphase domains, less than the length-scale of X-ray diffraction, prevents  $P2_1/c$  refinement in samples with composition  $\text{Di}_{59}\text{En}_{41}$  and  $\text{Di}_{52}\text{En}_{42}\text{CaTs}_2$ . The refined clinopyroxenes encompass the transition from  $P2_1/c$  to  $C2/c$  structures. In the  $P2_1/c$  structure, the  $A$  and  $B$  chains of tetrahedra undergo a slight straightening with increasing Ca content, and changes similar to those observed at high temperature. The results are in general agreement with large changes in the configuration of the chains at the transition, as observed during the  $P2_1/c - C2/c$  transition at high pressure and high temperature.

*Keywords:* phase transition, Rietveld refinement, clinopyroxene, crystal structure, diopside–enstatite join, average structure.

### SOMMAIRE

Nous avons affiné la structure de cinq compositions de clinopyroxène de la série entre diopside et enstatite en utilisant la méthode de Rietveld pour traiter les spectres de diffraction obtenus sur poudre avec rayonnement synchrotron. La fiabilité des résultats obtenus avec cette méthode a été vérifiée en les comparant avec les résultats antérieurs obtenus sur monocristal de l'échantillon de composition  $\text{Di}_{80}\text{En}_{20}$ ; la concordance est satisfaisante. Une différence dans la coordonnée  $y/b$  du site  $M2$  est liée à la plus faible résolution des données obtenues sur poudre dans ce travail, et notre inaptitude d'observer un dédoublement au site  $M2$ . L'analyse de Rietveld nous a permis de déceler les modulations sur (010) dues aux déformations du réseau précédant l'exsolution. La faible dimension des domaines antiphases primitifs, inférieure à l'échelle de résolution en diffraction X, entrave un affinement des compositions  $\text{Di}_{59}\text{En}_{41}$  et  $\text{Di}_{52}\text{En}_{42}\text{CaTs}_2$  dans le groupe d'espace  $P2_1/c$ . L'intervalle des compositions de clinopyroxène affinées couvre la transition structurale de  $P2_1/c$  à  $C2/c$ . Dans la structure  $P2_1/c$ , les chaînes de tétraèdres  $A$  et  $B$  se redressent légèrement à mesure qu'augmente la teneur en Ca, et simulent les changements observés à température élevée. Les résultats concordent en général avec les changements majeurs dans la configuration des chaînes lors de la transition  $P2_1/c - C2/c$  à pression et à température élevées.

(Traduit par la Rédaction)

*Mots-clés:* transition de phase, affinement de Rietveld, clinopyroxène, structure cristalline, série diopside–enstatite, structure moyenne.

<sup>§</sup> *E-mail addresses:* mario.tribaudino@unipr.it, fabrizio.nestola@uni-bayreuth.de, meneghini@fis.uniroma3.it

## INTRODUCTION

Structural changes and phase transformations in minerals as a function of composition, temperature and pressure have been widely studied to understand the evolution of crust and mantle assemblages. Among the major rock-forming minerals, pyroxenes have been the focus of several theoretical and experimental studies, most recently by Yang & Prewitt (2000), Downs (2003), and Thompson & Downs (2003, 2004).

In this paper, a set of clinopyroxene compositions ranging between  $\text{Di}_{20}\text{En}_{80}$  and  $\text{Di}_{80}\text{En}_{20}$  is investigated by synchrotron-radiation X-ray powder diffraction and Rietveld profile and structure-refinement analysis. Within this range, intermediate compositions are affected by small-size antiphase domains and strain preliminary to exsolution (Tribaudino 2000); moreover, site splitting at the  $M2$  site is present in samples unstrained and homogeneous at the scale of TEM observations. Our aims in the present investigation are to test Rietveld analysis for the highly defective intermediate Di–En clinopyroxenes and possibly to clarify the structural changes from the  $P2_1/c$  to the  $C2/c$  structures along the join; we will compare the results with those occurring at high pressures and high temperatures.

## BACKGROUND INFORMATION

A simplified model for mantle pyroxenes is provided by the system diopside–enstatite (Di–En,  $\text{CaMgSi}_2\text{O}_6$ – $\text{Mg}_2\text{Si}_2\text{O}_6$ ). Both orthorhombic and monoclinic pyroxenes are present along that join (Yang & Prewitt 2000). The orthorhombic varieties are limited to a narrow stability-field on the enstatite side (Gasparik 1990), whereas monoclinic pyroxenes are present along the whole join, with two space groups,  $P2_1/c$  and  $C2/c$ . At room temperature, the  $P2_1/c$  phase occurs in clinopyroxenes with less than 0.6 Ca atoms per formula unit, *apfu* (Tribaudino 2000), whereas the symmetry  $C2/c$  pertains to those those with a higher Ca content. At high temperature,  $P2_1/c$  pyroxenes undergo a phase transition to  $C2/c$  (Smyth 1969, Prewitt *et al.* 1971, Tribaudino *et al.* 2002, 2003a). The same transition, *i.e.*,  $P2_1/c$  to  $C2/c$  occurs with increasing pressure; it has been shown, however, that the high-pressure and high-temperature  $C2/c$  structures are very different (Angel *et al.* 1992, Tribaudino *et al.* 2001, Nestola *et al.* 2004). From a crystallographic point of view, the transition occurs as the two chains of tetrahedra, *A* and *B*, symmetrically independent in  $P2_1/c$ , become equivalent in the space group  $C2/c$ . Different structural mechanisms drive the transitions occurring with pressure, temperature and composition, in spite of the fact that in all cases the high-symmetry phase crystallizes in the space group  $C2/c$ . The high-pressure  $C2/c$  phase has a strongly kinked chain of tetrahedra, and the resulting structure can be interpreted on the basis of a distorted cubic close-packing of oxygen (Angel *et al.* 1992, Thompson

& Downs 2003); the high-temperature  $C2/c$  phase has instead elongate chains, and can be described on the basis of a distorted hexagonal packing of oxygen atoms. In the  $P2_1/c$  phase, the chains of tetrahedra have S and O rotations for the *A* and *B* chains, respectively (Yang & Prewitt 2000). These chains become O-rotated in the  $C2/c$  structures, after the HP and HT transitions. A first-order behavior was observed for both the high-temperature and the high-pressure  $P2_1/c \rightarrow C2/c$  transitions in clinopyroxene with a composition  $\text{Di}_{15}\text{En}_{85}$  (Tribaudino *et al.* 2002, Nestola *et al.* 2004).

The high-pressure and high-temperature phase transitions were used to obtain the thermal and compressional history of the host rocks (Bozhilov *et al.* 1999, Arlt *et al.* 2000). Whereas the structural mechanism and the thermodynamics of the high-pressure and high-temperature phase transitions are well described, fewer data exist on the structural and thermodynamic changes driven by compositional changes at room temperature from the  $P2_1/c$  to the  $C2/c$  structures. In fact, structural data along the diopside–enstatite join are available only for clinopyroxenes with Ca content lower than 0.23 (Ohashi & Finger 1976, Tribaudino & Nestola 2002) or higher than 0.66 *apfu* (Bruno *et al.* 1982, Tribaudino *et al.* 1989). The available data suggest that in the  $P2_1/c$  phase at room temperature, the chains of tetrahedra become similar with increasing Ca, as observed at high temperature. In the Ca-rich  $C2/c$  phase, the kink angle of the symmetry-unique chain of tetrahedra is intermediate between that of the high-pressure and high-temperature  $C2/c$  phase. The chain is O-rotated, and only minor changes in the kink angle occur with varying Ca content.

A structural investigation on intermediate Di–En clinopyroxenes has until now been hindered by the lack of crystals suitable for single-crystal analysis. Recent advances in structural determination *via* Rietveld powder-diffraction analysis has allowed us to overcome the lack of single crystals.

## EXPERIMENTAL

*Sample characterization*

Powder-diffraction patterns were made for six samples with composition (mol. %),  $\text{Di}_{80}\text{En}_{20}$ ,  $\text{Di}_{70}\text{En}_{30}$ ,  $\text{Di}_{59}\text{En}_{41}$ ,  $\text{Di}_{52}\text{En}_{46}\text{CaTs}_2$  (with CaTs representing the Ca-Tschermak component,  $\text{CaAl}_2\text{SiO}_6$ ),  $\text{Di}_{40}\text{En}_{60}$  and  $\text{Di}_{20}\text{En}_{80}$ . The samples with composition  $\text{Di}_{80}\text{En}_{20}$  and  $\text{Di}_{20}\text{En}_{80}$  were synthesized at room pressure, from a glass of  $\text{Di}_{80}\text{En}_{20}$  composition devitrified at 1230°C and room pressure for 225 h (Benna *et al.*, 1990), and by annealing a gel of  $\text{Di}_{20}\text{En}_{80}$  composition for 1440 h at  $T = 1375^\circ\text{C}$ ; the samples  $\text{Di}_{70}\text{En}_{30}$ ,  $\text{Di}_{59}\text{En}_{41}$ ,  $\text{Di}_{52}\text{En}_{46}\text{CaTs}_2$  and  $\text{Di}_{40}\text{En}_{60}$  were synthesized at high pressure, at conditions reported in Tribaudino *et al.* (2003a). All the samples studied were synthesized at hypersolvus conditions.

Apart from the sample  $\text{Di}_{80}\text{En}_{20}$ , which was also subject of single-crystal investigation (Tribaudino *et al.* 1989), all samples are composed of crystals smaller than a few  $\mu\text{m}$ , and hence all are unsuitable for single-crystal diffraction. The samples were further ground in an agate mortar before the powder-diffraction experiments.

Transmission electron microscopy (TEM) with energy-dispersion analysis showed that the sample  $\text{Di}_{20}\text{En}_{80}$  is homogeneous down to the nanoscale, as indicated by non-periodic contrast under TEM observation. In previous investigations, Rossi *et al.* (1987) and Tribaudino (2000) showed that  $\text{Di}_{80}\text{En}_{20}$  and  $\text{Di}_{70}\text{En}_{30}$  clinopyroxenes also are homogeneous, whereas the samples  $\text{Di}_{59}\text{En}_{41}$ ,  $\text{Di}_{52}\text{En}_{46}\text{CaTs}_2$ , and  $\text{Di}_{40}\text{En}_{60}$  display non-periodic modulations, mostly elongate almost parallel to (100) and (001) (Tribaudino 2000, Tribaudino *et al.* 2003a). In selected-area diffraction patterns, the modulations give rise to peak broadening, but no splitting of peaks indicative of coexistence of  $P2_1/c$  and  $C2/c$  phases with distinct composition was observed; the formation of satellite reflections, indicative of spinodal decomposition, also was not observed. Non-periodic compositional modulations in a single phase were found at the beginning of the exsolution process by Weinbruch *et al.* (2003) during the annealing of a pyroxene of composition  $\text{Di}_{54}\text{En}_{46}$ . The modulations in our samples, synthesized at hypersolvus conditions, are possibly formed as the sample crosses the two-phase field during cooling from a relatively high temperature or, alternatively, may be remnants of local clustering already present at hypersolvus conditions. The extent of the compositional difference between the modulations is not clear, their average distance being smaller than 50 Å, below the resolution of the available TEM–EDS system (400 Å). The presence of a spinodal decomposition mechanism for the exsolution in intermediate diopside–enstatite pyroxene, found by Weinbruch *et al.* (2003), would suggest very small compositional changes for samples in this work, which are at the very preliminary stages of exsolution.

Analysis of selected-area diffraction patterns shows the presence of  $b$ -type  $h + k$  odd reflections, indicative of a primitive lattice, assumed to be  $P2_1/c$ , in all grains in samples  $\text{Di}_{52}\text{En}_{46}\text{CaTs}_2$ ,  $\text{Di}_{40}\text{En}_{60}$  and  $\text{Di}_{20}\text{En}_{80}$ . These reflections are rather faint and elongate in sample  $\text{Di}_{52}\text{En}_{46}\text{CaTs}_2$ , very sharp in the others. In a few grains in sample  $\text{Di}_{59}\text{En}_{41}$ , faint  $h + k$  odd reflections were found as well. Minimum-spot TEM–EDS analytical results on sample  $\text{Di}_{59}\text{En}_{41}$ , described in a previous paper on TEM results (Tribaudino 2000), show that it is compositionally heterogeneous, consisting of grains with a composition between  $\text{Di}_{65}\text{En}_{35}$  and  $\text{Di}_{55}\text{En}_{45}$ , with a maximum frequency at  $\text{Di}_{59}\text{En}_{41}$ . Compositions with Ca content higher than 0.60 Ca *apfu* were invariably found to be associated with the absence of  $b$ -type reflections in the relevant electron-diffraction patterns (*i.e.*, with space group  $C2/c$ ), and those with lower Ca content, with  $P2_1/c$ . No evidence of a compositional gap

was found. The sharpness of  $b$ -type reflections is related to the size of the antiphase domains, rather than to strong structural differences. The size of the domains is of the order of 10 nm, with large C-centered boundaries (Weinbruch *et al.* 2003) in  $\text{Di}_{52}\text{En}_{46}\text{CaTs}_2$  and, where present, in  $\text{Di}_{59}\text{En}_{41}$ , of the order of a micrometer or more in samples poorer in Ca.

Conventional powder X-ray diffraction showed that in all the samples investigated, the only crystalline phase is a single clinopyroxene phase.

#### *Synchrotron-radiation powder-diffraction patterns*

The synchrotron-radiation powder-diffraction patterns used for Rietveld refinements were collected at the ESRF – BM8 GILDA beamline, using an angle-dispersive set-up based on an imaging plate (IP) camera and a fixed wavelength,  $\lambda = 0.61993$  Å. Details on the apparatus are reported in Meneghini *et al.* (2001). The sample  $\text{Di}_{52}\text{En}_{46}\text{CaTs}_2$  was collected also at  $\lambda = 0.55133$  Å, in order to obtain a higher-resolution pattern. Sample powders were enclosed in glass capillaries (inner diameter 0.5 mm) mounted horizontally on a goniometer head placed 300 mm from the IP. The capillaries were kept rotating during the acquisition in order to improve the grain statistics. The sample-to-image-plate distance and the instrumental line-shape were calibrated by refining the diffraction patterns of reference  $c$ -Si powders (NIST–SRM). The 2D diffraction patterns collected on the IP were digitized and integrated to standard one-dimensional diffraction patterns (intensity *versus*  $2\theta$ ). The maximum  $2\theta$  was  $\sim 50^\circ$  for sample  $\text{Di}_{52}\text{En}_{46}\text{CaTs}_2$  and  $43^\circ$  for the other samples.

#### *Rietveld refinements*

The diffraction patterns were quantitatively analyzed using the Rietveld refinement methods implemented in the GSAS (Larson & Von Dreele 1985) package. Background, overall scale-factor, unit-cell, line-shape parameters and March–Dollase preferred orientation were at first refined. The pseudo-Voigt profile function of Howard (1982) was used; the Lorentzian coefficient was expressed as  $\gamma = \gamma_0 \tan(\theta)$ , and the Gaussian variance of the peak, as  $\sigma^2 = \sigma_0^2$ . An asymmetry coefficient improved the fit of the peaks, and was refined together with  $\gamma_0$  and  $\sigma_0$ . A shifted Chebychev function with 12 parameters was used to model the background.

The presence or absence in the diffraction patterns of  $h + k$  odd reflections was used as criterion to chose the space group for the refinement. As shown in Figure 1, the (011) reflection is significantly present only in  $\text{Di}_{40}\text{En}_{60}$  and  $\text{Di}_{20}\text{En}_{80}$ . In samples  $\text{Di}_{52}\text{En}_{46}\text{CaTs}_2$  and  $\text{Di}_{59}\text{En}_{41}$ , the lack of the (011) reflection contrasts with TEM evidence. As a matter of fact, the intensity of  $b$ -type reflections in these samples is too faint to be revealed by powder diffraction. Because of the presence of a  $P2_1/c$  structure, without a sufficient information

to refine it, the structure of the  $\text{Di}_{52}\text{En}_{46}\text{CaTs}_2$  sample was not refined. In sample  $\text{Di}_{59}\text{En}_{41}$ , a  $C2/c$  refinement was done, averaging the contribution of locally  $P2_1/c$  grains, and the structure obtained has to be considered an average structure in a sample that is both compositionally and structurally inhomogeneous. Incidentally, the analysis of the strain with temperature showed for  $\text{Di}_{52}\text{En}_{46}\text{CaTs}_2$  and  $\text{Di}_{59}\text{En}_{41}$  a small but significant contribution of the spontaneous strain for the transition (Tribaudino *et al.* 2003). A  $C2/c$  space group was assigned to  $\text{Di}_{80}\text{En}_{20}$  and  $\text{Di}_{70}\text{En}_{30}$  samples.

In all samples, the  $M1$  and the  $T$  sites were assumed to be fully occupied by Mg and Si, respectively; all Ca was assumed to occupy the  $M2$  site, and the remainder of the  $M2$  site was modeled as Mg. During the first stages of refinement, coordinates and displacement parameters were fixed at the values determined by single-crystal refinements in  $\text{Di}_{80}\text{En}_{20}$  (Benna *et al.*

1990) and  $\text{Di}_{23}\text{En}_{77}$  (Tribaudino & Nestola 2002) for the  $C2/c$  and  $P2_1/c$  samples, respectively. Refinement of atom coordinates, and of isotropic displacement parameters for  $M2$  and  $O2$  (the latter only in the  $C2/c$  structures), was subsequently allowed. As in single-crystal-diffraction data, these displacement parameters were found to be very large, owing to significant positional disorder (see subsequent section). Their refinement was invariably positive definite, and the refined values decreased toward values for the end members, in agreement with the expectation of a decreased positional disorder.

To prevent unrealistic fluctuations in the coordinates of oxygen, the bond lengths in the tetrahedra were soft-constrained to the values determined by single-crystal structure refinements on  $\text{Di}_{80}\text{En}_{20}$  and  $\text{Di}_{23}\text{En}_{77}$  for the  $C2/c$  and  $P2_1/c$  samples, respectively. The strength of the constraints was progressively reduced during the late stages of the refinement, according to the procedure outlined in Nowell *et al.* (2002). During constrained refinement, a  $\psi^2_{\text{T}} = \psi^2_{\text{P}} + \psi^2_{\text{R}}$  function is minimized, with a  $\psi^2_{\text{P}}$  profile contribution and a  $\psi^2_{\text{R}}$  restraint contribution. The reduced  $\psi^2$  is given by  $\psi^2_{\text{T}}/(N_0 - P)$ , where  $N_0$  is the number of observations (number of restraints plus number of data points in the profile), and  $P$  is the number of variable parameters. Reduced  $\psi^2$  and  $\psi^2_{\text{R}}$  are reported in Table 1. To verify whether the imposed constraints can alter the coordinates of oxygen O3, and the O3–O3–O3 kink angle, which will be subject of a subsequent discussion, unconstrained refinements were also carried out. Such refinements, which ended with structure-agreement parameters close to the constrained refinement, gave unrealistic T–O bond lengths, but the differences from the O3–O3–O3 kink angle obtained after constrained and unconstrained refinements, although significant, are not of an extent such as to change the conclusions of the following structural discussion.

A correction for anisotropic strain-induced broadening was performed and significantly improved the fit in samples  $\text{Di}_{59}\text{En}_{41}$ ,  $\text{Di}_{52}\text{En}_{46}\text{CaTs}_2$ , and  $\text{Di}_{40}\text{En}_{60}$ . The resulting strain tensor is almost an ellipse lying on (010). This is in agreement with the presence of modulations parallel to (100) and (001) but not on (010), as found by TEM observations.

To test the actual precision of Rietveld results, the refinement was repeated, systematically varying the refinement procedure, *e.g.*, varying the profile coefficients, the compression factor and the  $2\theta$  range. Although the fit of the plot worsened during these attempts, the refined coordinates were not systematically different. It was found, however, in agreement with Hill (1982), that the observed differences are greater than the nominal standard deviation. The actual experimental uncertainty was found to be better represented by a  $5\sigma$  value.

In Figure 2, the fit between observed and calculated patterns is reported. Refinement parameters, atomic

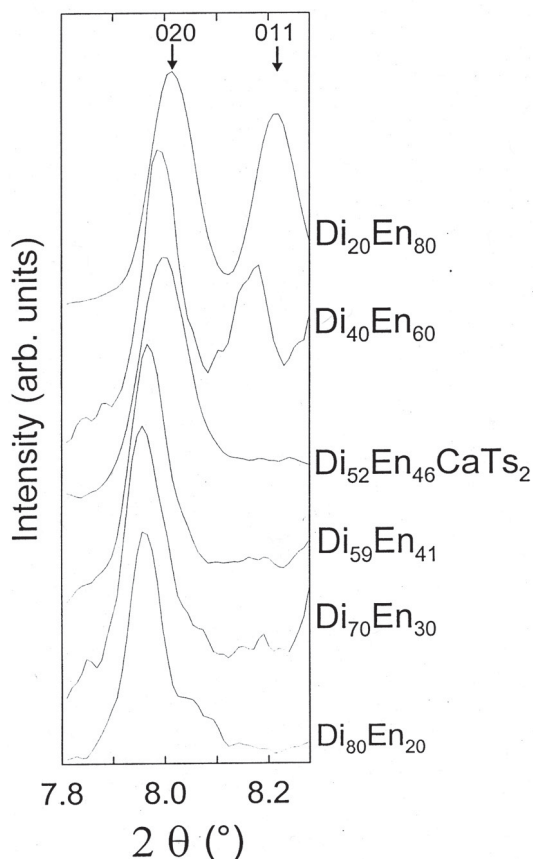


FIG. 1. The evolution of the (011) reflection in the samples examined.

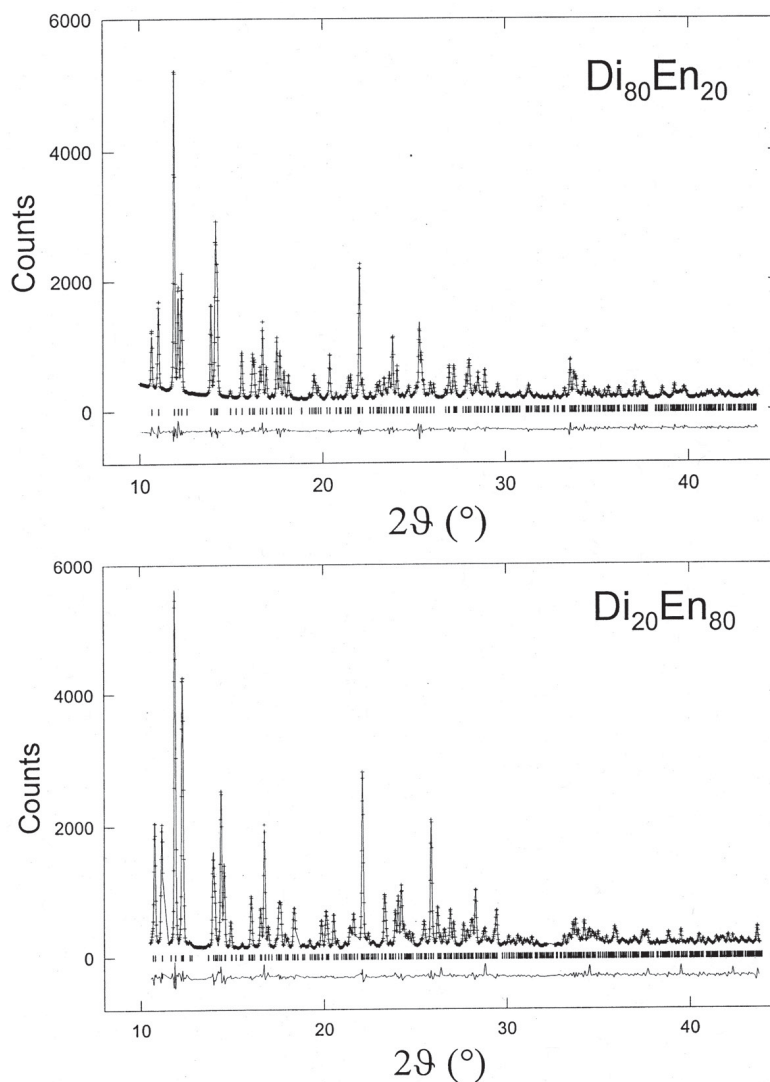


FIG. 2. Observed (crosses), calculated (solid line) and difference (lower solid line) profiles in powder-diffraction patterns of the refined  $\text{Di}_{80}\text{En}_{20}$  and  $\text{Di}_{20}\text{En}_{80}$  samples. Peak positions are indicated at the zero count level. The fits of the other patterns are available from the authors.

coordinates and displacement parameters, and bond lengths are reported in Tables 1, 2 and 3.

#### DISCUSSION

##### *Average and local structure*

Structural investigations along the Di-En join have been performed at different levels of detail in several

investigations. The crystal structure that can be obtained by refinement can be considered real only in the case of end members (Bruno *et al.* 1982, Ohashi 1984). In the refinement of intermediate solid-solutions between Ca-rich and Ca-poor clinopyroxenes, large displacement-parameters and significant residuals were observed. In most papers, these residuals are neglected (*e.g.*, Ohashi & Finger 1976), which affects the agreement factors very little with respect to other uncertainties

(compositional, microtextural), and average results are obtained. In some clinopyroxenes with intermediate Ca-content, these features prompted split-atom refinements at least of Ca and Mg at the  $M2$  site (Bruno *et al.* 1982, Rossi *et al.* 1987, Tribaudino *et al.* 1989, Tribaudino & Nestola 2002). The underlying physical rationale of such a model is the presence of a split of Ca and Mg in subsites at about 0.4 Å due to clustering prior to exsolution. A split was observed also for the O2 and O3 atoms, but should in principle be present for all atoms. These observations require high-resolution data collection, down to at least 0.4 Å resolution, corresponding in conventional single-crystal Mo source to a  $2\theta$  of about 90°. In this work, only average refinements were done; the resolution of the data is 0.85 Å (0.65 Å for  $\text{Di}_{52}\text{En}_{46}\text{CaTs}_2$ ), and the relatively low intensity and crowding of reflections with  $2\theta > 30^\circ$  make the extraction of reliable intensities more challenging than with single-crystal; data; the actual resolution may then be even lower than the nominal one.

The results of these refinements are, as discussed above, those of an average structure. These results, however, may refer to distinct situations:

1) the coexistence of local configurations with Ca or Mg in the  $M2$  site, in a sample homogeneous under TEM observation. This is the case of samples  $\text{Di}_{80}\text{En}_{20}$ ,  $\text{Di}_{70}\text{En}_{30}$ ,  $\text{Di}_{20}\text{En}_{80}$ . Local configurations could be revealed by the presence of significant residuals in the Fourier map at the end of structural refinement performed with high-resolution data, but from the powder-diffraction data in this work, the only suggestion comes from the larger value of the  $B_{M2}$  in  $\text{Di}_{70}\text{En}_{30}$  with respect to  $\text{Di}_{80}\text{En}_{20}$ .

2) the presence of clustering, which induces local strain, preliminary to exsolution, that is revealed by TEM observation of a non-periodic modulation; such strain induces a broadening of the diffraction pattern, *i.e.*, a broadening related to the orientation of the strain tensor, which does not affect all the reflections in the same way. This is the case of samples  $\text{Di}_{59}\text{En}_{41}$ ,  $\text{Di}_{52}\text{En}_{46}\text{CaTs}_2$  and  $\text{Di}_{40}\text{En}_{60}$ . The correction for anisotropic strain was significant only in these samples. A

further source of peak broadening, most effective in  $b$ -type reflections, comes from small-size antiphase domains. These occur in  $\text{Di}_{59}\text{En}_{41}$  and  $\text{Di}_{52}\text{En}_{46}\text{CaTs}_2$ , reducing the detectability of  $h + k$  odd reflections even below the background limit.

3) the coexistence of two chemically distinct phases, which give distinct diffraction-patterns. The critical points are the size of the phases, which have each to be larger than the length-scale for X-ray diffraction (a few hundred Å; Redfern 1996), and the difference in chemical composition. The latter point is important in that some chemical dispersion in analytical data is commonly found in results of electron-microprobe analysis of synthetic samples, and most commonly in intermediate pyroxenes along the diopside–enstatite join (*e.g.*, Lindsley & Dixon 1976). The case of an inhomogeneous composition of a single phase is obviously different from that of coexisting phases with different composition, like lamellae of pigeonite and augite. In the diffraction pattern in the former case, a broadening of single peaks exists, whereas in the latter, a splitting of peaks is present. The modulations observed by TEM in some pyroxenes of this work are about 50 Å in size, *i.e.*, smaller than the X-ray length-scale. As a consequence, the diffraction patterns, both by TEM and powder diffraction, in these modulated phases are those of a single clinopyroxene, albeit with broader diffraction-peaks. The average composition of the modulated clinopyroxenes studied in this work has some dispersion, and is therefore inhomogeneous, but without a bimodal distribution of the composition (Tribaudino 2000). For the samples studied here, TEM evidence rules out the coexistence of chemically distinct phases, which, however, are easily found in natural pigeonite (Tribaudino *et al.* 2003b).

4) the coexistence of crystallographically distinct phases, here  $P2_1/c$  and  $C2/c$ , irrespective of a strong chemical difference. In natural exsolved pyroxenes, a chemical difference also is present. In this work, analytical data for sample  $\text{Di}_{59}\text{En}_{41}$  alone would indicate an inhomogeneous single phase, and only the TEM crystallographic analysis shows the presence of

TABLE 1. UNIT-CELL PARAMETERS AND RESULTS OF REFINEMENT OF CLINOPYROXENES ALONG THE JOIN Di–En

Crystal	$\text{Di}_{80}\text{En}_{20}$	$\text{Di}_{70}\text{En}_{30}$	$\text{Di}_{59}\text{En}_{41}$	$\text{Di}_{52}\text{En}_{46}\text{CaTs}_2$	$\text{Di}_{40}\text{En}_{60}$	$\text{Di}_{20}\text{En}_{80}$
$a$ (Å)	9.7323(2)	9.7264(3)	9.7110(6)	9.7084(4)	9.7042(4)	9.6655(2)
$b$ (Å)	8.9152(2)	8.9133(3)	8.8935(6)	8.8802(4)	8.8805(4)	8.8534(2)
$c$ (Å)	5.2464(1)	5.2485(2)	5.2452(3)	5.2475(2)	5.2423(3)	5.2138(1)
$\beta$ (°)	106.357(1)	106.742(3)	107.278(5)	107.523(5)	108.084(4)	108.349(2)
$V$ (Å <sup>3</sup> )	436.785(8)	432.73(2)	432.56(4)	431.41(2)	429.45(2)	423.48(1)
reduced $\chi^2$	0.769	0.676	2.471	1.220	0.667	1.964
$\chi^2_{\text{R}}$	10.0	1.0	25.3	-	7.5	1.3
$R_{\text{p}}$ (%)	3.6	3.3	6.2	4.6	3.2	5.0
$R_{\text{wp}}$ (%)	4.8	4.6	8.4	6.3	4.6	7.4
$\text{RF}^2$ (%)	7.2	8.8	12.5	-	21.5	9.2

$P2_1/c$  and  $C2/c$ . In the presence of crystallographically coexisting distinct phases, a splitting of peaks in the powder-diffraction pattern could be seen only in the presence of sufficiently large changes in cell parameters, and such were not observed in  $\text{Di}_{59}\text{En}_{41}$ .

#### Comparison with single-crystal data

A test was done comparing Rietveld to single-crystal data for sample  $\text{Di}_{80}\text{En}_{20}$ , which was taken from the same synthesis run used for previous single-crystal

room-temperature and high-temperature investigations (Tribaudino *et al.* 1989, Benna *et al.* 1990), and the only one for which single-crystal data are available. The coordinates are in reasonable agreement, with differences less than those observed in an analogous comparison for diopside (Raudsepp *et al.* 1990); the only significant difference between structural models obtained by Rietveld and single-crystal refinements is the  $y/b$  coordinate of  $M2$ . This coordinate is supposedly reliable, being very stable during several tests on powder-diffraction data; it systematically displays a value different from that for the single crystal (0.294 versus 0.298).

The Fourier density along the diad axis was therefore calculated from Rietveld and single-crystal data across the  $M2$  site (Fig. 3). A larger and more symmetrical peak is present in Rietveld than in the single-crystal refinement. The Fourier profile of the single crystal comes from the presence of a Ca site, a stronger scatterer, coexisting with a smaller contribution for Mg, at about 0.4 Å from the main peak, which results in an asymmetrical peak and a shoulder. The maximum of the  $M2$  peak corresponds almost to the position of Ca, and cuts off the shoulder related to Mg, revealed

TABLE 2. FRACTIONAL COORDINATES AND ISOTROPIC DISPLACEMENT PARAMETERS OF ATOMS IN CLINOPYROXENES ALONG THE JOIN Di–En

atoms	$x/a$	$y/b$	$z/c$	$B_{\text{iso}}$
$\text{Di}_{80}\text{En}_{20}$				
$M2$	0	0.29449(26)	0.25	0.52(6)
$M1$	0	0.90659(41)	0.25	0.47
$T$	0.28784(19)	0.09317(24)	0.23405(34)	0.39
$O1$	0.11572(29)	0.08818(56)	0.1442(7)	0.51
$O2$	0.36344(42)	0.24968(34)	0.3269(7)	0.41(6)
$O3$	0.34865(41)	0.01881(35)	-0.0021(6)	0.65
$\text{Di}_{70}\text{En}_{30}$				
$M2$	0	0.2885(4)	0.25	1.14(10)
$M1$	0	0.9053(6)	0.25	0.47
$T$	0.28957(30)	0.09409(32)	0.2387(6)	0.39
$O1$	0.11741(30)	0.08969(51)	0.1468(10)	0.51
$O2$	0.36522(46)	0.25009(41)	0.3337(12)	0.35(16)
$O3$	0.35009(51)	0.01811(14)	0.0030(6)	0.65
$\text{Di}_{59}\text{En}_{41}$				
$M2$	0	0.2839(7)	0.25	1.33(18)
$M1$	0	0.9068(9)	0.25	0.47
$T$	0.2902(4)	0.0929(4)	0.2444(8)	0.39
$O1$	0.1168(4)	0.08933(76)	0.1445(15)	0.51
$O2$	0.3665(6)	0.25055(58)	0.3301(19)	0.73(17)
$O3$	0.3514(7)	0.02117(24)	0.0077(9)	0.65
$\text{Di}_{40}\text{En}_{60}$				
$M2$	0.2546(18)	0.0244(8)	0.2309(29)	0.66(22)
$M1$	0.2515(13)	0.6543(10)	0.2411(24)	0.62
$TA$	0.0411(11)	0.3449(10)	0.2730(20)	0.58
$O1A$	0.8655(12)	0.3360(26)	0.1522(33)	0.51
$O2A$	0.1091(20)	0.5109(15)	0.3087(43)	0.80
$O3A$	0.0933(16)	0.2675(16)	0.5723(23)	1.31
$TB$	0.5522(12)	0.8429(12)	0.2484(22)	0.67
$O1B$	0.3771(13)	0.8372(26)	0.1442(31)	0.79
$O2B$	0.6314(20)	0.9937(15)	0.3826(35)	1.32
$O3B$	0.6009(19)	0.7116(17)	0.4836(24)	1.12
$\text{Di}_{20}\text{En}_{80}$				
$M2$	0.2555(8)	0.0186(4)	0.2279(13)	0.34(10)
$M1$	0.2517(8)	0.6536(6)	0.2275(12)	0.62
$TA$	0.0420(4)	0.3418(5)	0.2842(8)	0.58
$O1A$	0.8664(4)	0.3392(15)	0.1764(18)	0.51
$O2A$	0.1159(10)	0.5042(7)	0.3169(19)	0.80
$O3A$	0.1038(7)	0.2746(8)	0.5941(10)	1.31
$TB$	0.5498(5)	0.8392(6)	0.2301(9)	0.67
$O1B$	0.3738(5)	0.8356(16)	0.1305(18)	0.79
$O2B$	0.6332(11)	0.9847(8)	0.3803(20)	1.32
$O3B$	0.6067(9)	0.7064(8)	0.4677(12)	1.12

Unrefined displacement parameters (shown without associated errors) were taken from the single-crystal data for  $\text{Di}_{80}\text{En}_{20}$  (Benna *et al.* 1990) and  $\text{Di}_{23}\text{En}_{77}$  (Tribaudino & Nestola 2002) for the  $C2/c$  and  $P2_1/c$  structures, respectively.

TABLE 3. SELECTED BOND-DISTANCES (Å) AND ANGLES (°) IN CLINOPYROXENES ALONG THE JOIN Di–En

	$\text{Di}_{80}\text{En}_{20}$	$\text{Di}_{70}\text{En}_{30}$	$\text{Di}_{59}\text{En}_{41}$	$\text{Di}_{40}\text{En}_{60}$	$\text{Di}_{20}\text{En}_{80}$
$M2-O1A$	2.305(5)	2.257(5)	2.227(8)	2.231(29)	2.129(12)
$M2-O1B$				2.173(30)	2.135(13)
$M2-O2A$	2.278(4)	2.227(5)	2.220(8)	2.247(29)	2.153(12)
$M2-O2B$				1.991(26)	1.987(12)
$M2-O3A$	2.612(4)	2.628(4)	2.657(6)	2.398(18)	2.312(9)
$M2-O3B$				2.899(19)	2.981(10)
$M2-O3C$	2.777(4)	2.824(4)	2.841(6)	2.641(18)	2.536(8)
$M2-O3A$				3.471(20)	3.563(10)
$\langle M2-O \rangle 6 O$	2.398	2.371	2.368	2.280	2.209
$\langle M2-O \rangle 8 O$	2.493	2.484	2.486	2.506	2.474
$M1-O2A$	2.046(4)	2.039(6)	2.028(8)	1.990(12)	2.019(10)
$M1-O2B$				2.050(12)	2.045(12)
$M1-O1A$	2.058(3)	2.067(5)	2.043(7)	2.024(13)	2.056(11)
$M1-O1B$				2.087(12)	2.063(11)
$M1-O1A$	2.133(5)	2.157(6)	2.145(9)	2.144(14)	2.148(13)
$M1-O1B$				2.183(14)	2.150(13)
$\langle M1-O \rangle$	2.079	2.088	2.072	2.083	2.080
$TA-O2A$	1.588(2)	1.585(1)	1.588(1)	1.602(3)	1.590(1)
$TA-O1A$	1.608(2)	1.604(1)	1.608(1)	1.625(4)	1.612(1)
$TA-O3A$	1.655(2)	1.660(1)	1.655(1)	1.642(3)	1.647(1)
$TA-O3A$	1.674(2)	1.674(1)	1.674(1)	1.641(5)	1.665(1)
$\langle TA-O \rangle$	1.631	1.631	1.632	1.628	1.628
$TB-O2B$				1.595(7)	1.589(1)
$TB-O1B$				1.616(5)	1.615(1)
$TB-O3B$				1.656(8)	1.670(1)
$TB-O3B$				1.671(5)	1.677(1)
$\langle TB-O \rangle$				1.634	1.638
$O3A-O3A-O3A$	165.4(3)	166.0(1)	163.7(2)	193.5(1.2)	199.0(6)
$O3B-O3B-O3B$				150.8(1.2)	147.0(6)
$O3A-O3A-O3A^*$	165.5(3)	167.0(5)	169.3(7)	194.4(1.3)	198.8(7)
$O3B-O3B-O3B^*$				154.8(1.5)	146.7(8)

Site nomenclature according to Burnham *et al.* (1967). \* unconstrained refinement.

in single-crystal refinement by a peak in the difference-Fourier map (Bruno *et al.* 1982). The Rietveld data do not allow us to resolve the two peaks, and give a space average and a displaced position of the peak. This affects the individual  $M2-O$  bond lengths, which are systematically different from those obtained with single-crystal data, whereas the average  $M2-O$  bond lengths are very similar.

In other refined samples, single-crystal data are not available for comparison with Rietveld results. However for any given structural parameter, a trend consistent with that of single-crystal data could be outlined, as shown in Figure 4 for the average  $M2-O$  bond lengths.

#### Structural changes from $P2_1/c$ to $C2/c$ clinopyroxenes

The transition from the  $P2_1/c$  to  $C2/c$  structures in the Di-En join and in the related Hd-Fs join (Ohashi *et al.* 1975) is driven by the increase in the average size of the  $M2$  cation, due to Ca-for-Mg substitution, which is also responsible for the changes in the  $M2$  polyhedron, the configuration of the chains of tetrahedra, and the overall increase in unit-cell volume along the join. Thompson & Downs (2004) showed that the transition can be simply modeled on the basis of changes in the chains of tetrahedra, whose extension is measured

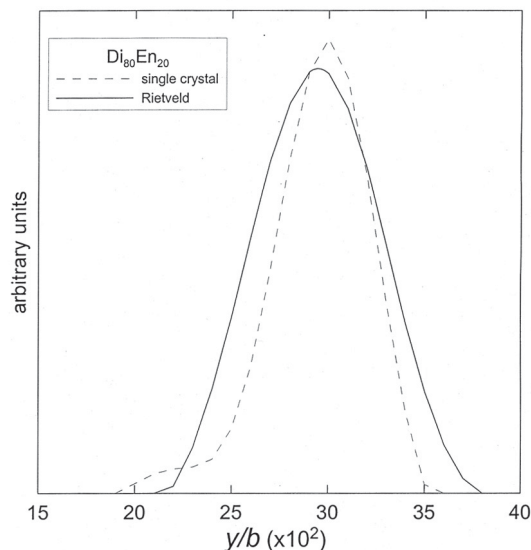


FIG. 3. Profile of the electron density in a Fourier calculation along the  $b$  axis through the  $M2$  site, at  $x/a = 0$  and  $z/c = 0.25$ , on the basis of refinements of data from powder diffraction (this work) and single-crystal diffraction (Tribaudino *et al.* 1989).

by the O3-O3-O3 kink angle. The kink angles are measured assuming a common reference-direction for both chains (Thompson & Downs 2004). For the  $B$  chain, this leads to values less than  $180^\circ$ , but for the  $A$  chain, which is rotated in the opposite direction, it leads to values greater than  $180^\circ$ . With increasing Ca content in  $P2_1/c$  clinopyroxenes, both chains straighten, *i.e.*, the angle becomes closer to  $180^\circ$ . After the transition, only minor changes in the kink angle of the unique chain in  $C2/c$  are observed as a function of composition. The evolution of the kink angles of  $A$  and  $B$  chains with increasing Ca content is outlined in Figure 5.

Thompson & Downs (2004) showed that in the structure of a given pyroxene, the straightening of the chain of tetrahedra increases the cell volume. Therefore, an extension in the  $A$  and  $B$  chains, which decreases the difference in the kink angle, can be predicted at high temperature or with increasing size of the  $M2$  cation, in order to increase the cell volume with temperature or composition. In the  $P2_1/c$  clinopyroxene  $Di_{15}En_{85}$  (Tribaudino *et al.* 2002), the  $A$  and  $B$  chains each straighten by about  $7^\circ$  between 25 and  $1000^\circ\text{C}$ . Incidentally, in the structure of  $P2_1/c$  clinopyroxene  $Di_{15}En_{85}$  under pressure, the volume must decrease, and the  $A$  and  $B$  chains of tetrahedra inflect by  $1.5$  and  $3^\circ$ , respectively, between room and 4.5 GPa (Nestola *et al.* 2004).

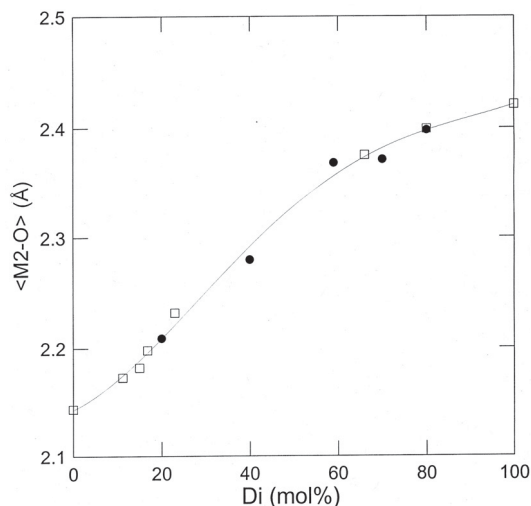


FIG. 4. Average  $M2-O$  bond length calculated on the basis of six oxygen atoms along the join Di-En; open squares refer to single-crystal refinements, full dots to Rietveld refinements (this work). A polynomial trend is given for reference. Data for single crystals: Ohashi (1984) for clinoenstatite, Ohashi & Finger (1976) for  $Di_{11.2}En_{88.8}$  and  $Di_{16.8}En_{83.2}$ , Tribaudino & Nestola (2002) for  $Di_{15}En_{85}$  and  $Di_{23}En_{77}$ , Tribaudino *et al.* (1989) for  $Di_{66}En_{34}$  and  $Di_{80}En_{20}$ , and Bruno *et al.* (1982) for diopside.

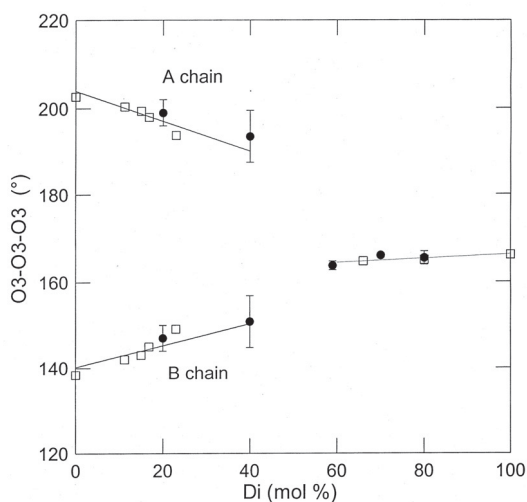


FIG. 5. Variation in O3–O3–O3 kink angle of tetrahedra with composition for the  $P2_1/c$  (left) and  $C2/c$  (right) clinopyroxenes. Symbols as in Figure 3. For Rietveld data, the reported error is five times the nominal error.

Although data are still lacking for the compositions between  $\text{Di}_{40}\text{En}_{60}$  and  $\text{Di}_{60}\text{En}_{40}$ , the present data along the join Di–En in going from  $P2_1/c$  to  $C2/c$  structures follow a trend in agreement with structural changes in  $P2_1/c$  and  $C2/c$  phases before and after the high-temperature phase transition (Smyth 1974, Sueno *et al.* 1984, Arlt & Armbruster 1997, Tribaudino *et al.* 2002, Cámara *et al.* 2002). An increase in the  $M2$  polyhedron and cell volume due to increasing cation-size or to increasing vibration of the  $M2$  cation is observed in both cases in  $P2_1/c$  structures before the transition. It must, however, be noted that the difference between the  $A$  and  $B$  chains of tetrahedra in the  $P2_1/c$  structure decreases little with temperature, and a strong first-order change occurs in order to achieve the  $C2/c$  configuration (Tribaudino *et al.* 2002). A large change also has to occur close to the  $\text{Di}_{60}\text{En}_{40}$  composition, as suggested by inspection of the  $P2_1/c$  and  $C2/c$  phase fields (Fig. 6).

The present data along the join and the apparent discontinuous behavior at the transition with temperature (Fig. 6) are in agreement with the general view of a sharp change at the transition, although they are not sufficient to rule out a more continuous behavior. In a continuous behavior, however, at a given composition (about  $\text{Di}_{60}\text{En}_{40}$ , by linear extrapolation of the data on O3–O3–O3 kinking angles in  $P2_1/c$ ), the two different chains of the primitive structure close to the transition should display the same sense of rotation. This could occur only by an inflection of the  $A$  chain in hypothetical Ca-rich  $P2_1/c$  structure, and would promote a decrease in the cell volume (Thompson & Downs

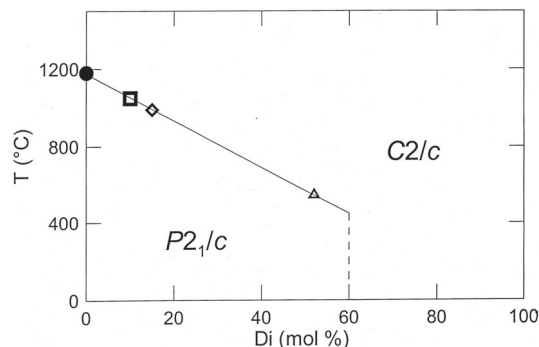


FIG. 6.  $P2_1/c$  –  $C2/c$  phase fields in the Di–En join. Data from: Shimobayashi & Kitamura (1991) for clinoenstatite (full circle), Schwab & Schwerin (1975) for  $\text{Di}_{10}\text{En}_{90}$  (open square), Tribaudino *et al.* (2002) for  $\text{Di}_{15}\text{En}_{85}$  (open diamond, untreated homogeneous sample), and Tribaudino *et al.* (2003a) for  $\text{Di}_{52}\text{En}_{46}\text{CaTs}_2$  (open triangle). The phase boundary is a mere indication for the reader and is not based on a specific thermodynamic model.

2004). Further Ca-for-Mg substitution and the related increase in volume would then not be possible in the  $P2_1/c$  structure. The  $C2/c$  phase is therefore more stable, and the transition takes place, in agreement with the experimental lack of intermediate  $P2_1/c$  structures with an O-rotated  $A$  chain.

#### ACKNOWLEDGEMENTS

Helpful comments and suggestions by Joseph Smyth, Dana Griffen, Giancarlo Della Ventura and an anonymous referee significantly improved the paper. This work was supported by MIUR (project: “Phase transitions and order–disorder processes in minerals”).

#### REFERENCES

- ANGEL, R.J., CHOPELAS, A. & ROSS, N.L. (1992): Stability of high-density clinoenstatite at upper mantle pressures. *Nature* **358**, 322–324.
- ARLT, T. & ARMBRUSTER, T. (1997): The temperature-dependent  $P2_1/c$ – $C2/c$  phase transition in the clinopyroxene kanoite  $\text{MnMg}[\text{Si}_2\text{O}_6]$ : a single crystal X-ray and optical study. *Eur. J. Mineral.* **9**, 953–964.
- \_\_\_\_\_, KUNZ, M., STOLTZ, J., ARMBRUSTER, T. & ANGEL, R.J. (2000): P–T–X data on  $P2_1/c$  clinopyroxenes and their displacive phase transitions. *Contrib. Mineral. Petrol.* **138**, 35–45.
- BENNA, P., TRIBAUDINO, M., ZANINI, G. & BRUNO, E. (1990): The crystal structure of  $\text{Ca}_{0.8}\text{Mg}_{1.2}\text{Si}_2\text{O}_6$  clinopyroxene ( $\text{Di}_{80}\text{En}_{20}$ ) at  $T = -130^\circ, 25^\circ, 400^\circ$  and  $700^\circ$  C. *Z. Kristallogr.* **192**, 183–199.

- BOZHILOV, K.N., GREEN, H.W., II & DOBRZHINETSAYA, L. (1999): Clinoenstatite in Alpe Arami peridotite: additional evidence of very high pressure. *Science* **284**, 128-132.
- BRUNO, E., CARBONIN, S. & MOLIN, G.M. (1982): Crystal structure of Ca-rich clinopyroxenes on the  $\text{CaMgSi}_2\text{O}_6$ - $\text{Mg}_2\text{Si}_2\text{O}_6$  join. *Tschermaks Mineral. Petrogr. Mitt.* **29**, 223-240.
- BURNHAM, C.W., CLARK, J.R., PAPIKE, J.J. & PREWITT, C.T. (1967): A proposed crystallographic nomenclature for clinopyroxene structure. *Z. Kristallogr.* **125**, 109-119.
- CÁMARA, F., CARPENTER, M.A., DOMENEGHETTI, M.C. & TAZZOLI, V. (2002): Non-convergent ordering and displacive phase transition in pigeonite: in-situ HT XRD study. *Phys. Chem. Minerals* **29**, 331-340.
- DOWNES, R.T. (2003): Topology of the pyroxenes as a function of temperature, pressure and composition as determined from the procrystal electron density. *Am. Mineral.* **88**, 556-566.
- GASPARIK, T. (1990): A thermodynamic model for the enstatite–diopside join. *Am. Mineral.* **75**, 1080-1091.
- HILL, R.J. (1992): Rietveld refinement round robin. I. Analysis of standard X-ray and neutron data for  $\text{PbSO}_4$ . *J. Appl. Crystallogr.* **25**, 589-610.
- HOWARD, C.J. (1982): The approximation of asymmetric neutron powder diffraction peaks by sums of gaussians. *J. Appl. Crystallogr.* **15**, 615-620.
- LARSON, A.C. & VON DREELE, R.B. (1985): *GSAS – General Structure Analysis System*. Los Alamos National Laboratory, Los Alamos, New Mexico.
- LINDSLEY D.H. & DIXON, S.A. (1976): Diopside–enstatite equilibria at 850 to 1400°C, 5 to 35 kb. *Am. J. Science* **276**, 1285-1301.
- MENEGHINI, C., ARTIOLI, G., BALERNA, A., GUALTIERI, A.F., NORBY, P. & MOBILIO, S. (2001): A translating imaging plate system for in-situ experiments at the GILDA beamline. *J. Synchr. Rad.* **8**, 1162-1166.
- NESTOLA, F., TRIBAUDINO, M. & BOFFA BALLARAN, T. (2004): High pressure behavior, transformation and crystal structure of synthetic iron-free pigeonite. *Am. Mineral.* **89**, 189-196.
- NOWELL, H., ATTFIELD, J.P. & COLE, J.C. (2002): The use of restraints in Rietveld refinement of molecular compounds; a case study using the crystal structure determination of the tryptamine free base. *Acta Crystallogr.* **B58**, 835-840.
- OHASHI, Y. (1984): Polysynthetically-twinned structures of enstatite and wollastonite. *Phys. Chem. Minerals* **10**, 217-229.
- \_\_\_\_\_, BURNHAM, C.W. & FINGER, L.W. (1975): The effect of Ca–Fe substitution on the clinopyroxene crystal structure. *Am. Mineral.* **60**, 423-434.
- \_\_\_\_\_ & FINGER, L.W. (1976): The effect of Ca substitution on the structure of clinoenstatite. *Carnegie Inst. Wash., Year Book* **75**, 743-746.
- PREWITT, C.T., BROWN, G.E. & PAPIKE, J.J. (1971): Apollo 12 clinopyroxenes: high temperature X-ray diffraction studies. *Geochim. Cosmochim. Acta, Suppl.* **2**, 1, 59-68.
- RAUDSEPP, M., HAWTHORNE, F.C. & TURNOCK, A.C. (1990): Evaluation of the Rietveld method for the characterisation of fine-grained products of mineral synthesis: the diopside–hedenbergite join. *Can. Mineral.* **28**, 93-109.
- REDFERN, S.A.T. (1996): Length scale dependence of high-pressure amorphization: the static amorphization of anorthite. *Mineral. Mag.* **60**, 493-498.
- ROSSI, G., OBERTI, R., DAL NEGRO, A., MOLIN, G.M. & MELLINI, M. (1987): Residual electron density of the M2 site in  $C2/c$  clinopyroxenes: relationships with bulk chemistry and sub-solidus evolution. *Phys. Chem. Minerals* **14**, 514-520.
- SCHWAB, R.G. & SCHWERIN, M. (1975): Polimorphie und Entmischungsreaktionen der Pyroxene im System Enstatit ( $\text{MgSiO}_3$ ) – Diopsid ( $\text{CaMgSi}_2\text{O}_6$ ). *Neues Jahrb. Mineral., Abh.* **124**, 223-245.
- SHIMOBAYASHI, N. & KITAMURA, M. (1991): Phase transition in Ca-poor clinopyroxenes: a high temperature transmission electron microscopic study. *Phys. Chem. Minerals* **18**, 153-160.
- SMYTH, J.R. (1969): Orthopyroxene high–low clinopyroxene inversions. *Earth Planet. Sci. Lett.* **6**, 406-407.
- \_\_\_\_\_ (1974): The high temperature crystal chemistry of clinohypersthene. *Am. Mineral.* **59**, 1069-1082.
- SUENO, S., KIMATA, M. & PREWITT, C.T. (1984): The crystal structure of high clinoferrosilite. *Am. Mineral.* **69**, 265-269.
- THOMPSON, R.M. & DOWNES, R.T. (2003): Model pyroxenes. I. Ideal topologies. *Am. Mineral.* **88**, 653-666.
- \_\_\_\_\_ & \_\_\_\_\_ (2004): Model pyroxenes. II. Structural variation as a function of tetrahedral rotation. *Am. Mineral.* **89**, 614-628.
- TRIBAUDINO, M. (2000): A transmission electron microscope investigation on the  $C2/c$ – $P2_1/c$  phase transition in clinopyroxenes along the diopside–enstatite ( $\text{CaMgSi}_2\text{O}_6$ – $\text{Mg}_2\text{Si}_2\text{O}_6$ ) join. *Am. Mineral.* **85**, 707-715.
- \_\_\_\_\_, BENNA, P. & BRUNO, E. (1989): Average structure and M2 site configurations in  $C2/c$  clinopyroxenes along the Di–En join. *Contrib. Mineral. Petrol.* **103**, 452-456.
- \_\_\_\_\_ & NESTOLA, F. (2002): Average and local structure in  $P2_1/c$  clinopyroxenes along the join diopside–enstatite ( $\text{CaMgSi}_2\text{O}_6$ – $\text{Mg}_2\text{Si}_2\text{O}_6$ ). *Eur. J. Mineral.* **14**, 549-555.

- \_\_\_\_\_, \_\_\_\_\_, CÁMARA, F. & DOMENEGHETTI, M.C. (2002): The high temperature  $P2_1/c$ – $C2/c$  phase transition in Fe-free pyroxene ( $\text{Ca}_{0.15}\text{Mg}_{1.85}\text{Si}_2\text{O}_6$ ): structural and thermodynamic behavior. *Am. Mineral.* **87**, 648–657.
- \_\_\_\_\_, \_\_\_\_\_, MENEGHINI, C. & BROMILEY, G.D. (2003a): The high temperature  $P2_1/c$ – $C2/c$  phase transition in Fe-free Ca-rich  $P2_1/c$  clinopyroxenes. *Phys. Chem. Minerals* **30**, 527–535.
- \_\_\_\_\_, PASQUAL, D., MOLIN, G.M. & SECCO, L. (2003b): Microtextures and crystal chemistry in  $P2_1/c$  pigeonites. *Mineral. Petrol.* **77**, 161–176.
- \_\_\_\_\_, PRENCIPE, M., NESTOLA, F. & HANFLAND, M. (2001): A  $P2_1/c$ – $C2/c$  high pressure phase transition in  $\text{Ca}_{0.5}\text{Mg}_{1.5}\text{Si}_2\text{O}_6$  clinopyroxene. *Am. Mineral.* **86**, 807–813.
- WEINBRUCH, S., STYRSA, V. & MÜLLER, W.F. (2003): Exsolution and coarsening in iron-free clinopyroxene during isothermal annealing. *Geochim. Cosmochim. Acta* **67**, 5071–5082.
- YANG, HEXIONG & PREWITT, C.T. (2000): Chain and layer silicates at high temperatures and pressures. In *High Temperature and High Pressure Crystal Chemistry* (R.M. Hazen & R.T. Downs, eds.). *Rev. Mineral. Geochem.* **41**, 211–255.

Received September 24, 2004, revised manuscript accepted June 24, 2005.